Cl'+HCl(v=1, j=3)→Cl'H(v', j')+Cl reaction dynamics over an extended collision energy range

Pamela M. Aker and John P. Fulmer

Citation: The Journal of Chemical Physics **99**, 244 (1993); doi: 10.1063/1.466219
View online: http://dx.doi.org/10.1063/1.466219
View Table of Contents: http://scitation.aip.org/content/aip/journal/jcp/99/1?ver=pdfcov
Published by the AIP Publishing

$Cl'+HCl(v=1, j=3)\rightarrow Cl'H(v', j')+Cl$ reaction dynamics over an extended collision energy range

Pamela M. Aker
Department of Chemistry, University of Pittsburgh, Pittsburgh, Pennsylvania 15260

John P. Fulmer
Department of Chemistry, University of Wisconsin–Milwaukee, Milwaukee, Wisconsin 53201

(Received 16 February 1993; accepted 26 March 1993)

Quasiclassical trajectory calculations have been used to model the $Cl'+HCl(v=1, j=3)\rightarrow Cl'H(v', j')+Cl$ exchange reaction dynamics over the 0–1.5 eV collision energy range. A kinematic constraint, which results from the H+LH mass combination, forces the reaction to strongly conserve initial vibrational excitation, independent of collision energy. This kinematic constraint is weaker than forces induced by the reaction potential anisotropy however, for the reaction does not strongly conserve initial rotational excitation. Reaction proceeds via two mechanisms which are classified as direct (single H atom exchange) and indirect (multiple H atom exchanges). Approximately 30% of the reaction proceeds via indirect exchange, independent of collision energy.

I. INTRODUCTION

Studies of the dynamics of H+LH exchange reactions have undergone a recent renaissance. Reactive resonances in the symmetric I+HI, Br+HBr, and Cl+HCl systems have been identified in the photodetachment spectroscopy experiments of Neumark *et al.*,[1–5] and corresponding theoretical studies have confirmed (or corrected) the transition state vibrational mode assignments.[6–11] The theoretical studies have also shown that resonances in H+LH reactions are amenable to probing via "ordinary" reaction dynamics experiments.[11–15] For example, in the Cl+HCl exchange reaction, both differential and integral cross sections are strongly influenced by resonances; there is a sudden switch to sideways scattering, and a smooth steplike increase in the integral cross section when the collision energy of the system is tuned over a resonance. This behavior survives summing over all partial waves in the system, a very exciting result, since it means that it may be more feasible to experimentally detect resonance signatures in H+LH systems, as compared with the $H+H_2$ system, which requires a probing of rotational state-to-state differential cross sections.

In addition to transition state resonances, the H+LH exchange reaction dynamics are influenced by kinematic effects.[16–24] Collinear dynamics studies (both quantum and quasiclassical) show that reactivity oscillates quite strongly when the collision energy of the system is varied. The oscillations arise because the 1D collision complex lifetimes are principally determined by the relative velocity of the two heavy atoms in the system. If the two heavy atoms approach, repel, and separate in a time which corresponds to a half number of intermediate H–L–H asymmetric vibrations (an odd number of light atom exchanges) then reaction takes place. If the collision time corresponds to an integer number of vibrations (an even number of light atom exchanges), then no reaction occurs.

Quasiclassical trajectory (QCT) calculations show that reactivity oscillations survive in three dimensions, but only if certain types of potential energy surfaces are used in the simulations. In their detailed studies on the $Cl'+HCl\rightarrow Cl'H+Cl$ and $O+HCl\rightarrow OH+Cl$ reactions, Persky *et al.* have shown that COLD surfaces (those that direct the reactants toward a collinear geometry and form rotationally "cold" products) give oscillations in product state distributions and differential cross sections.[19–23] In addition, it was shown that reactant HCl vibration and rotation strongly influences the magnitude of the observed oscillations, in the former case there is an enhancement, in the latter a diminution. In contrast, HREP surfaces, (those that are repulsive in nature and form products with a high degree of rotational excitation), show extremely weak oscillations only for $HCl(v\geqslant 1)$, and no oscillatory structure for reaction from the ground vibrational level.

Since reactivity oscillations are strongly influenced by the nature of the surface governing the reaction, their experimental detection will provide an extremely sensitive probe of true reaction potential. As the calculations mentioned above were done using a restricted range of reactant orientation angle and impact parameter, the authors suggested that an oriented moleculer beam scattering experiment would be the best vessel for exploring reactivity oscillations. However, these types of experiments are difficult and an easier experiment would be one that simply detects variations in product state distributions as a function of reactant collision energy.

In the following, we outline extensive QCT calculations on the reaction $Cl'+HCl(v=1, j=3)\rightarrow Cl'H(v', j')+Cl$. We have simulated the reaction dynamics over a wide range of energy to determine if reactivity oscillations are present for this particular HCl reactant rovibrational state, since it is one which can be easily prepared via stimulated Raman pumping. In addition we have done the QCT calculations using a Monte Carlo sampling of reactant orientation angles and impact parameters such that we mimic conditions found in a bulb-type experiment. We have chosen to follow this procedure for two reasons. First,

 0021-9606/93/99(1)/244/10/$6.00

the calculations fully similate experimental conditions, and second, because previous work has focused only on small reactant angle and impact parameter, we wanted to see if the 3D reactivity oscillations survived conditions of full convergence.

II. METHOD

Muckerman's QCT program was used to model the dynamics of Cl+HCl(v=1, j=3) collisions.[25] Calculations were run over two different collision energy regimes defined as overall (0–1.5 eV in 0.1 eV steps), and threshold (0–0.50 eV in 0.01 eV steps). 300 000 trajectories were run at each collision energy. Energy was conserved to 1 in 10 000 and a maximum impact parameter, b_{max}, of 5 Å ensured that the calculations fully converged in all reaction channels.

The Persky and Kornweitz LEPS surface III (PK3) was used in the QCT calculations.[19] Although this potential is not the most accurate, we have chosen to use it in this study because it provides the optimum opportunity to probe classical reactivity oscillations. Marked oscillations in product differential cross sections, and mild oscillations in product energy partitioning, have been seen in previous 3D QCT calculations on this surface. However these calculations were done using j=0 reactant HCl and a limited range of reactant impact parameters and orientations. The purpose of this study is to see if the oscillations survive using input conditions that would be used in a real experiment, i.e., j=3 reactant HCl, and a complete Monte Carlo average of input orientations and impact parameters. Although we do expect a damping of oscillatory behavior by using reactant HCl in j=3, if the oscillations do survive they will be most prominent for the PK3 surface. Hence the results presented here provide an upper bound for observing reactivity oscillations.

Reactant and product parameters are defined as follows. The total cross section, σ_{tot}, for a reaction channel is given by $(N_{react}/N_{tot})\pi b_{max}^2$, where N_{react} is the number of trajectories that reacted, N_{tot} is the total number of energy conserving trajectories, and b_{max} is the maximum impact parameter. The vibrational, rotational, and translational energy partitioning values are given by $f_v' = \langle E_{vib}'\rangle/E_{tot}$, $f_r' = \langle E_{rot}'\rangle/E_{tot}$, and $f_t' = 1 - f_v' - f_r'$, respectively, where E_{vib}' and E_{rot}' are the product classical vibrational and rotational energies calculated by the trajectory program. Partial reaction cross sections are defined as $\sigma_{v'} = \pi b_{max}^2 N_{react,v'}/N_{tot}$, and differential cross sections as $d\sigma(\theta') = N(\theta')\pi b_{max}^2/(2\pi \sin\theta' \Delta\theta' N_{tot})$, where $N(\theta')$ is the number of trajectories in the reaction channel of interest that have scattered into a bin, $\Delta\theta'$, 20° wide with θ' the value of the angle at the midpoint of the bin. The opacity function, $P(b)$, is defined as $N_{react,b}/N_{tot,b}$ where $N_{react,b}$ is the number of trajectories reacted with impact parameter b in the channel of interest and $N_{tot,b}$ is the total number of trajectories with impact parameter b.

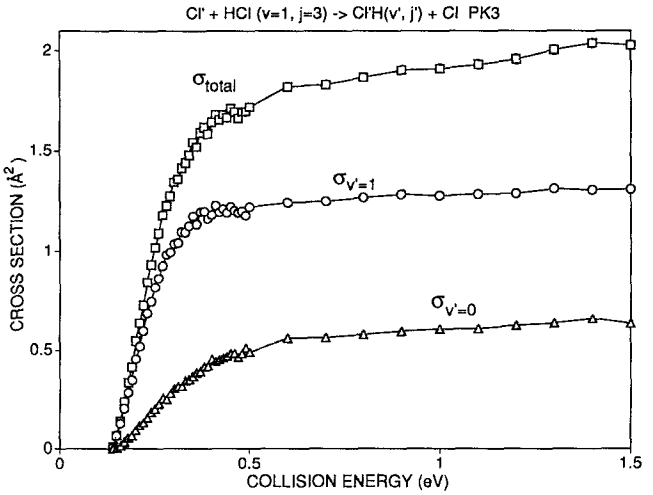

FIG. 1. Cl′+HCl(v=1, j=−3)→Cl′H(v', j')+Cl total and partial reaction cross sections calculated as a function of reactant collision energy. Error bars are hidden beneath the symbols.

III. RESULTS

The total cross sections calculated for the Cl′+HCl(v=1, j=3) exchange reaction over the collision energy range 0–1.5 eV are shown in Fig. 1 and listed in Table I. An inspection of Fig. 1 shows that the exchange reaction energy dependence closely resembles a step function. There is an extremely sharp increase in reactivity in the threshold energy regime—the cross section increases from 0.009 ±0.001 Å^2 at 0.14 eV to 1.71±0.02 Å^2 at 0.45 eV—but at energies higher than this the cross section rises only minimally, reaching to just 2.03±0.02 Å^2 at 1.5 eV collision energy. The reactivity energy dependence in the threshold energy regime does not follow the quadratic form predicted by an angle-dependent line-of-centers model.[26] Persky and Kornweitz have noted however that the strong anisotropic forces associated with the PK3 surface cause the reagents to reorient to a near collinear configuration at the time of reaction.[19] So a line-of-centers description cannot be used with this particular potential energy surface.

It is interesting to note that the exchange reaction cross section is quite small, <2 Å^2, even at collision energies well above the reaction barrier. Small cross sections have also been measured and calculated for the 1.6 eV H+HX→H$_2$+X(X=I, Cl, and Br) reactions.[27] In these latter reactions, low reaction probability results from a simple geometric constraint—the magnitude of the cross section is limited by the size of the H atoms in the system. A potential-independent "shell model of reactivity" was developed for the H+HX→H$_2$+X reactions, and the opacity functions and total reaction cross sections calculated using this model agreed well with their respective QCT calculated values.[27] It is not unreasonable to imagine that a similar geometric constraint exists in the Cl+HCl system, at least at high collision energies. However the total cross section predicted by the shell model (calculated with a saddle point Cl–H bond distance of 1.5 Å which corresponds to the outer turning point of the HCl v=1 vibration), 1.3 Å^2, is 35% smaller than the QCT calculated

TABLE I. Reaction cross sections for Cl′+HCl(v=1, j=3) →Cl′H(v'=0–2, j')+Cl.

E_{col} (eV)	σ_{tot}	$\langle v' \rangle$	$\sigma_{v'=0}$	$\sigma_{v'=1}$	$\sigma_{v'=2}$
0.14	0.009(1)	0.81	0.002(1)	0.007(1)	
0.15	0.065(4)	0.95	0.003(1)	0.062(4)	
0.16	0.138(6)	0.91	0.013(2)	0.125(6)	
0.17	0.233(8)	0.86	0.032(2)	0.201(7)	
0.18	0.334(9)	0.84	0.052(4)	0.281(9)	
0.19	0.41(1)	0.85	0.063(4)	0.35(1)	
0.20	0.54(1)	0.83	0.091(5)	0.45(1)	
0.21	0.64(1)	0.81	0.117(6)	0.52(1)	
0.22	0.73(1)	0.82	0.132(6)	0.59(1)	
0.23	0.84(1)	0.81	0.156(6)	0.69(1)	
0.24	0.93(2)	0.80	0.185(7)	0.74(1)	
0.25	1.02(2)	0.80	0.201(7)	0.82(1)	
0.26	1.09(2)	0.79	0.224(8)	0.86(1)	0.0003(3)
0.27	1.18(2)	0.79	0.254(8)	0.92(1)	0.002(1)
0.28	1.23(2)	0.80	0.246(8)	0.98(2)	0.001(1)
0.29	1.27(2)	0.79	0.277(9)	0.99(2)	0.004(1)
0.30	1.34(2)	0.77	0.305(9)	1.03(2)	0.003(1)
0.31	1.36(2)	0.77	0.315(9)	1.04(2)	0.004(1)
0.32	1.41(2)	0.78	0.315(9)	1.09(2)	0.005(1)
0.33	1.44(2)	0.76	0.344(9)	1.09(2)	0.004(1)
0.34	1.48(2)	0.76	0.35(1)	1.12(2)	0.004(1)
0.35	1.54(2)	0.76	0.37(1)	1.17(2)	0.005(1)
0.36	1.52(2)	0.75	0.38(1)	1.13(2)	0.005(1)
0.37	1.59(2)	0.76	0.39(1)	1.19(2)	0.006(1)
0.38	1.62(2)	0.75	0.41(1)	1.20(2)	0.006(1)
0.39	1.58(2)	0.74	0.42(1)	1.16(2)	0.009(2)
0.40	1.64(2)	0.73	0.45(1)	1.18(2)	0.009(2)
0.41	1.68(2)	0.74	0.44(1)	1.23(2)	0.012(2)
0.42	1.65(2)	0.73	0.45(1)	1.19(2)	0.010(2)
0.43	1.68(2)	0.73	0.46(1)	1.21(2)	0.012(2)
0.44	1.66(2)	0.72	0.47(1)	1.19(2)	0.008(2)
0.45	1.71(2)	0.72	0.48(1)	1.22(2)	0.010(2)
0.46	1.69(2)	0.72	0.48(1)	1.20(2)	0.009(2)
0.47	1.66(2)	0.73	0.46(1)	1.19(2)	0.009(2)
0.48	1.69(2)	0.72	0.48(1)	1.20(2)	0.013(2)
0.49	1.70(2)	0.70	0.51(1)	1.17(2)	0.010(2)
0.50	1.72(2)	0.72	0.49(1)	1.22(2)	0.010(2)
0.60	1.82(2)	0.70	0.56(1)	1.24(2)	0.018(2)
0.70	1.83(2)	0.70	0.56(1)	1.25(2)	0.018(2)
0.80	1.87(2)	0.70	0.58(1)	1.27(2)	0.022(2)
0.90	1.90(2)	0.70	0.59(1)	1.28(2)	0.028(3)
1.00	1.91(2)	0.70	0.60(1)	1.28(2)	0.031(3)
1.10	1.93(2)	0.71	0.61(1)	1.28(2)	0.041(3)
1.20	1.96(2)	0.71	0.62(1)	1.29(2)	0.046(3)
1.30	2.00(2)	0.71	0.63(1)	1.31(2)	0.059(4)
1.40	2.04(2)	0.72	0.66(1)	1.30(2)	0.071(4)
1.50	2.03(2)	0.74	0.63(1)	1.31(2)	0.081(5)

TABLE II. Reaction cross sections for Cl′+HCl(v=1, j=3) →Cl′H(v'=3–5, j')+Cl.

E_{col} (eV)	$\sigma_{v'=3}$	$\sigma_{v'=4}$	$\sigma_{v'=5}$
0.80	<0.001		
0.90	<0.001		
1.00	<0.001		
1.10	0.001(1)	<0.001	
1.20	0.001(1)	···	
1.30	<0.001	<0.001	
1.40	0.003(1)	0.001(1)	
1.50	0.004(1)	0.002(1)	<0.001

total cross section. This observation provides further evidence that potential anisotropy strongly influences Cl +HCl exchange reaction dynamics, and shows that increased reactivity results from reagent reorientation during the reaction.

Inspection of Fig. 1 shows that there are no oscillations in the total reaction cross sections as a function of collision energy. This result agrees with that predicted by Persky *et al.*,[19–23] but does contrast somewhat with coupled channel hyperspherical (CCH) calculations done using the PK3 surface.[16] The CCH calculations for Cl′+HCl(v=1, j=3)→Cl′H(v', j')+Cl show that there is a reactivity oscillation at 0.35 eV collision energy (0.71 eV total energy). However the CCH calculations were done only for total angular momentum J=0. This may explain the discrepancy with our results.

The QCT calculated partial vibrational reaction cross sections, $\sigma_{v'}$, for the HCl product v'=0 and 1 levels are also shown in Fig. 1, and listed in Table I. Both vibrational levels are populated at all collision energies studied, and the $\sigma_{v'}$ vs E_{col} plots resemble the step function seen for the total cross section, i.e., there is a sharp increase in population at low collision energy and a subsequent leveling off at high collision energy. Product HCl v'=2, 3, 4, and 5 levels are also accessed for reaction at collision energies above 0.25, 0.8, 1.1, and 1.5 eV, respectively, but reaction into these levels is extremely inefficient. As Table I shows, the v'=2 partial reaction cross section reaches only to 0.08 Å^2 at 1.5 eV collision energy. The cross sections for population into v'=3, 4, and 5 are even more minuscule. As shown in Table II, they are all <0.004 Å^2.

The Cl′+HCl exchange reaction shows a strong propensity to retain initial reagent vibrational excitation, a result expected from kinematic constraints imposed by the mass combination.[14,17,24] The partial reaction cross sections for v'=0 are at least a factor of 2 smaller than those for v'=1, at all collision energies studied. This aspect of the reaction dynamics is further emphasized by the $\langle v' \rangle$'s calculated for the reaction, which are listed in Table I. At 0.15 eV collision energy the $\langle v' \rangle$ is large, being 0.95. Between 0.15 and 0.5 eV collision energy the $\langle v' \rangle$ monotonically decreases, and then the value levels off around 0.7 at collision energies higher than 0.5 eV.

Results of limited reagent orientation QCT studies on the Cl+HCl(v=1, j=0) and O+HCl(v=1, j=0) reactions have lead Persky and Kornweitz to suggest that oscillations in the $P(v'=1)/P(v'=0)$ ratio in back scattered (170°–180°) products will occur, independent of the nature of the surface used in the study.[23] Statistical noise hampers our ability to say anything meaningful about this ratio in this particular angular range, but we have examined the global $P(v'=0$ and $1)$ values, where $P(v') = N_{v',exch}/N_{tot,exch}$. Plots of $P(v'=0)$ and $P(v'=1)$ vs collision energy are shown in Fig. 2(a) and a plot of the ratio of these two numbers in Fig. 2(b). Some intriguing spikes can be seen in these plots, specifically there is a sharp increase in $P(v'=1)$, a sharp decrease in $P(v'=0)$, and a corresponding spike in the $P(v'=1)/P(v'=0)$ ratio at 0.15 eV collision energy, relative to reaction at 0.14 eV.

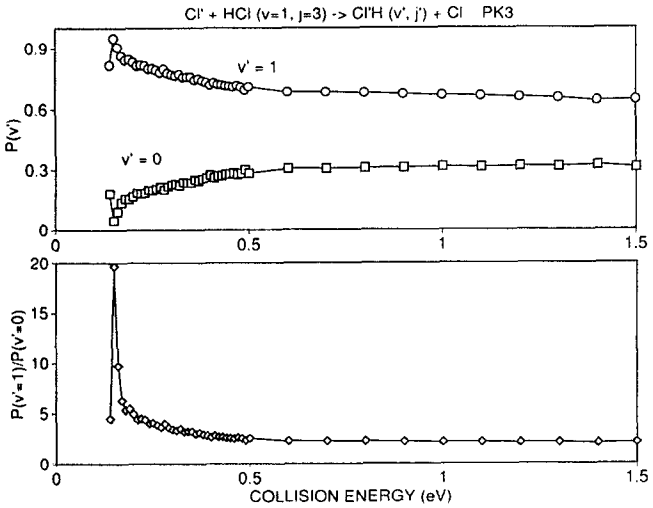

FIG. 2. Relative vibrational population distributions calculated for the Cl′+HCl (v=1, j=3) exchange reaction. The top panel plots $P(v'=0)$ and $P(v'=1)$ as a function of collision energy, the lower panel plots $P(v'=1)/P(v'=0)$.

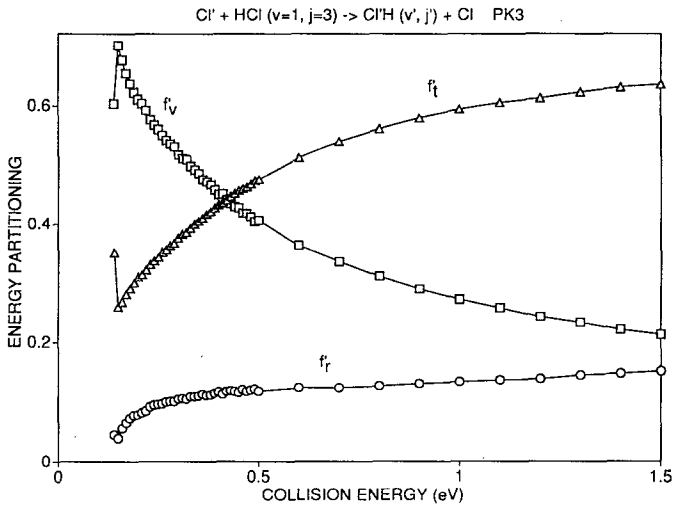

FIG. 3. Vibrational, rotational, and translational energy partitioning calculated in the Cl′+HCl(v=1, j=3)→Cl′H(v', j')+Cl reaction as a function of energy. Error bars have been omitted for clarity.

Excitement reigns for but a moment though, for these spikes are simple manifestations of the statistical error in the calculations done at 0.14 eV collision energy. In sum total only 33 trajectories out of a total of 300 000 reacted at this latter energy and the errors associated with the $P(v'=0$ and 1) values are 40% and 20%, respectively. If one ignores the noise-induced oscillatory structure then one sees that in general there is a small decrease in $P(v'=1)$, a corresponding small increase in $P(v'=0)$, and a slight drop in the $P(v'=1)/P(v'=0)$ ratio as the collision energy is changed from 0.15 to 0.5 eV. At collision energies higher than 0.5 eV the three values remain essentially stable, at 0.68, 0.3, and 2.1, respectively.

The limited impact parameter and reactant orientation QCT studies of Persky *et al.* also show that oscillations in back scattered (170°–180°) product vibrational, rotational, and translational energies, $\langle E'_v\rangle$, $\langle E'_r\rangle$, $\langle E'_t\rangle$, occur for reaction on the PK3 surface.[19–23] The error bars on the energy partitioning in this specific angular range are too large to make a meaningful observation, but we have looked to see if the global reaction f'_v, f'_r, and f'_t values oscillate as a function of collision energy; they do not. The f' values calculated for the 0–1.5 eV collision energy exchange reaction are shown in Fig. 3. The results show that the vibrational and translational energy partitioning are highly interdependent. The f'_v value starts out large, ~0.7 at 0.15 eV, but decreases monotonically as the collision energy is increased, until a value of ~0.2 is reached for reaction at 1.5 eV collision energy. The translational energy partitioning is opposite in behavior. Initially f'_t is small, ~0.25 at 0.15 eV, but this value increases as the collision energy increases, reaching ~0.6 at 1.5 eV. The large changes in the translational and vibrational energy partitioning do not mirror large changes in the reaction dynamics however. As noted above, the $P(v'=0$ and 1) and $\langle v'\rangle$ values change only slightly in the threshold energy (0–0.5 eV) regime, showing that there is a strong propensity for the reaction to conserve initial reagent vibrational excitation, i.e., $E_{v'}=E_v$. Most of the change in f'_v and f'_t is simply a reflection of the change in the fraction $E_{\text{vib,reactant}}/E_{\text{tot}}$, where $E_{\text{tot}}\sim E_{\text{vib,reactant}}+E_{\text{col}}$.

Previous studies show that the rule $j\rightarrow j'=j$ is followed in H+LH systems, albeit in the absence of a potential energy surface.[24] If this rule is closely followed in the Cl+HCl(v=1, j=3) exchange reaction, then we would expect the f'_r value to decrease as the collision energy is increased because $E_{j=3}/E_{\text{tot}}$ decreases. Figure 3 shows the exact opposite. The QCT calculated f'_r value increases with increasing collision energy, and the change is quite significant. At 0.15 eV f'_r is only ~0.04, at 1.5 eV it is ~0.15, an almost fourfold increase.

The peaks of the exchange product rotational state distributions, j'_{peak}, do shift to higher j' with increasing collision energy, but this shift is very minimal and does not contribute much to the change in f'_r. Table III lists the j'_{peak}'s calculated for the $v'=0$ and 1 levels of the exchange reaction product as a function of collision energy. In the $v'=1$ level the peak moves only 3 $\hbar$, from $j'=3$ to 6, as the collision energy is increased from 0.14 to 1.5 eV. A slightly larger shift occurs in the $v'=0$ level, at 0.14 eV the peak of the distribution is at $j'\sim 10$, at 1.5 eV $j'_{\text{peak}}=18$, but the energy change associated with this shift small because the HCl rotational constant is small and because only 30% of the reaction populates the $v'=0$ level.

Most of the change in f'_r is due to the substantial broadening of the rotational state distributions which arises when the reaction collision energy is increased. This is reflected in the $\langle j'\rangle$'s for the product $v'=0$ and 1 levels which are also listed in Table III. For reaction at 0.14 eV, the $\langle j'\rangle$'s in the $v'=0$ and 1 levels are 9.7 and 2.6, respectively. At 1.5 eV collision energy these values have increased substantially, to 19.1 and 11.6, respectively. To further illustrate the rotational broadening which occurs when the collision energy is increased, we have plotted the

TABLE III. Rotational energy disposal in Cl′+HCl(v=1, j=3) →Cl′H(v', j')+Cl.

E_{col} (eV)	$\langle j' \rangle_{v'=0}$	$j'_{peak,v'=0}$	$\langle j' \rangle_{v'=1}$	$j'_{peak,v'=1}$
0.14	9.7	na	2.6	3
0.15	9.5	na	3.2	3
0.16	10.8	10	3.5	3
0.17	11.3	11	3.6	3
0.18	11.6	11	3.6	3
0.19	11.9	12	3.8	3
0.20	11.9	13	4.0	3
0.21	12.1	13	4.0	3
0.22	12.2	13	4.1	3
0.23	12.3	12	4.4	3
0.24	12.2	13	4.5	3
0.25	12.5	13	4.4	3
0.26	12.6	13	4.6	3
0.27	12.4	13	4.7	3
0.28	12.6	13	4.9	3
0.29	12.5	12	4.8	3
0.30	12.7	12	4.9	3
0.31	12.9	13	4.9	3
0.32	12.9	13	5.0	3
0.33	13.0	13	5.2	3
0.34	13.0	13	5.1	3
0.35	13.0	13	5.2	3
0.36	13.1	13	5.3	3
0.37	13.2	13	5.3	3
0.38	13.3	14	5.3	4
0.39	13.2	14	5.3	4
0.40	13.3	14	5.5	3
0.41	13.4	15	5.5	3
0.42	13.5	14	5.6	4
0.43	13.5	14	5.6	3
0.44	13.5	14	5.6	3
0.45	13.6	13	5.6	3
0.46	13.8	14	5.7	3
0.47	13.7	15	5.8	3
0.48	13.7	15	5.9	3
0.49	13.8	14	5.9	4
0.5	13.7	14	5.9	3
0.6	14.5	16	6.4	4
0.7	14.8	16	6.4	4
0.8	15.0	16	7.5	3
0.9	15.6	16	8.1	3
1.0	16.0	17	8.6	4
1.1	16.6	17	9.2	3
1.2	16.7	16	9.6	5
1.3	17.4	17	10.5	6
1.4	17.4	19	11.0	6
1.5	19.1	18	11.6	5

v'=1 and 0 rotational state distributions calculated for reaction at 0.25 and 1.0 eV collision energy in Figs. 4(a) and 4(b), respectively. The 0.25 eV collision energy v'=1 product rotational state distribution is strongly peaked at j'=3 with a full-width at half-maximum (FWHM) of only 5 states (showing a propensity for $j \rightarrow j'=j$), and a j'_{max} of 13. The 1.0 eV collision energy product v'=1 distribution is much broader, the FWHM is 15 states and j'_{max} = 22, but the peak still occurs at low j', specifically at j'=4. Figure 4(b) shows that the 0.25 eV collision energy v'=0 product distribution is almost as strongly peaked as in the v'=1 level, the FWHM of the former, which peaks at j'=13, is only 7 states and j'_{max} is only 19. At 1.0 eV

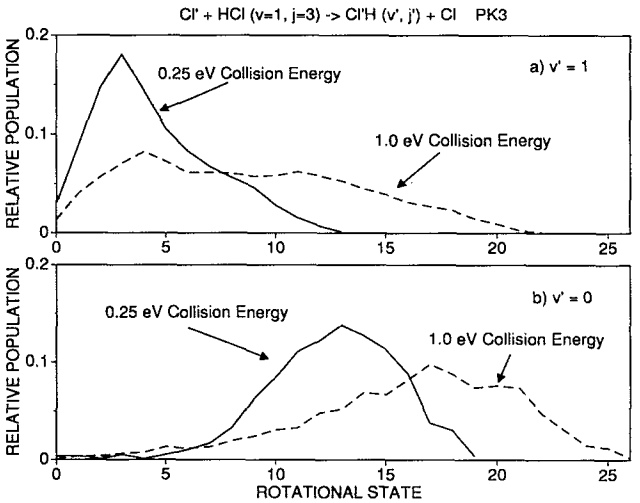

FIG. 4. Cl′+HCl(v=1, j=3) exchange reaction v'=1 and 1 product rotational state distributions calculated for reaction at 0.25 and 1.0 eV collision energy. Error bars are not shown.

collision energy the FWHM of the v'=0 distribution has increased to 10 states, the peak has shifted to 17, and j'_{max} is 26.

That the exchange reaction's $\langle j' \rangle$'s and f'_r's increase with increasing collision energy shows that forces exerted by the potential energy surface have more influence on the reaction dynamics than the mass induced kinematic constraints which dictate that $l \rightarrow l'=l$ and $j \rightarrow j'=j$. Obviously the potential influences the dynamics such that there is some interconversion between l and j'. Of course, since $l=\mu v_{rel} b$ the increase in product rotational excitation directly reflects the increase in l which occurs as v_{rel} is increased. But an examination of the opacity functions shows that increased product rotational excitation also stems from reaction at larger impact parameter which occurs when the reagent collision energy is increased. Figure 5 shows the exchange reaction opacity functions calculated

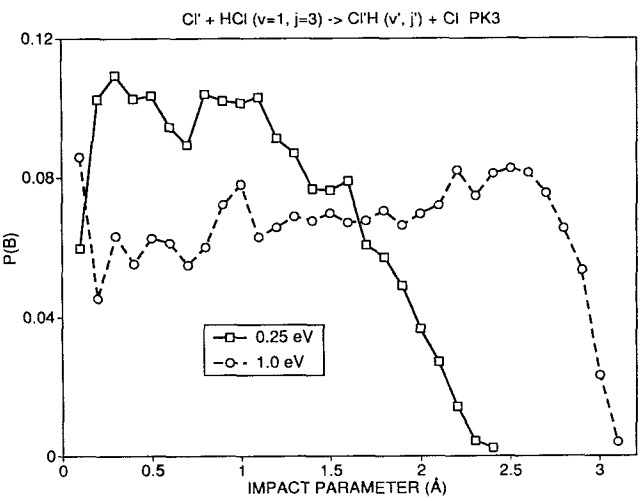

FIG. 5. Cl′+HCl(v=1, j=3) exchange reaction opacity functions calculated for reaction at 0.25 and 1.0 eV collision energy.

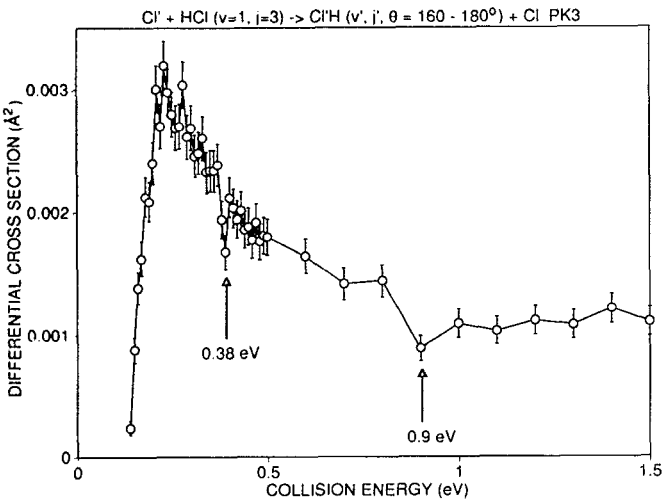

FIG. 6. Cl′+HCl(v=1, j=3) exchange reaction product center-of-mass differential cross sections calculated for scattering into the 160°–180° angular range.

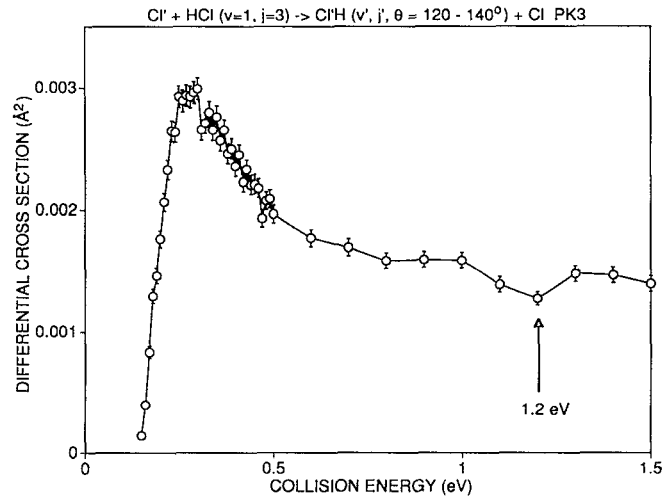

FIG. 7. Cl′+HCl(v=1, j=3) exchange reaction product center-of-mass differential cross sections calculated for scattering into the 120°–140° angular range.

for reaction at 0.25 and 1.0 eV collision energy. Although both opacity functions are steplike in character, the breadth of the low collision energy opacity function is narrower than the high collision energy one. The maximum impact parameter leading to reaction at 0.25 eV collision energy is 2.4 Å and the largest $P(b)$'s occur with $b < 1.5$ Å. The b_{max} for reaction at 1.0 eV collision energy is much greater, 3.1 Å, and reaction is, within the statistical error, equally probable for impact parameters up to ~2.7 Å.

Reactivity oscillations seen in the limited reactant orientation and impact parameter QCT calculations of Persky and Kornweitz were most prominent in the back scattered differential cross sections.[19–23] We have examined these cross sections in great detail and see some interesting structure, but it is difficult to say whether this structure is real because it appears just outside of the statistical error of the calculations. Figures 6 and 7 show plots of the differential cross section calculated as a function of collision energy for the exchange reaction product scattered into the 160°–180° and 120°–140° angular ranges, respectively, The error bars in these plots correspond to two standard deviations.

Figure 6 highlights two dips in reactivity which occur in product scattered into the 160°–180° angular range. The first dip, which is only 0.02 eV wide, is present at 0.38 eV collision energy. The second dip appears at 0.9 eV collision energy. We cannot determine the exact width of the 0.9 eV dip as calculations at the higher collision energies were done using a 0.1 eV grid. It is interesting to note that the lower collision energy dip observed in our calculations appears at an energy close to the 0.35 eV collision energy reactivity oscillation seen in Schatz's CCH (J=0) calculations on the Cl′+HCl(v=0, j=0) system,[16] and at an energy close to the 8 kcal mol^{-1} (0.35 eV) dip in backscattered product (170°–180°) that Persky and Kornweitz observed for reaction of the HCl(v=1, j=0, $\theta_{orientation}$ =30°) state on the PK4 surface.[22] But since the magnitudes of the dips seen in our calculations are just outside of the statistical error we cannot make a definitive statement about their reality. We leave the decision up to the reader.

No oscillatory structure was seen in the differential cross sections for scattering into the 140°–160° range, but as Fig. 7 shows, a small dip in reactivity is seen for reaction into the 120°–140° range at 1.2 eV collision energy. This dip in reactivity is shallower than the dips seen for reaction into the 160°–180° range, and again appears just outside of the statistical error.

We did examine the energy dependence of the differential cross sections calculated for scattering into all other angles but as the structure in these ranges is very smooth we do not present the results. The energy dependence of the exchange reaction angular distributions follows an expected general trend. Backscattering dominates at low collision energy. Product is increasingly forward scattered as the collision energy is increased, and at high collision energy the product is almost exclusively forward scattered. Figure 8 demonstrates this trend by showing the QCT calculated angular distributions arising from the 0.25, 0.6, and 1.5 eV collision energy exchange reactions.

IV. DISCUSSION

Single dimension (i.e., collinear) trajectory calculations on H+LH exchange reactions show pronounced oscillatory structure in the reaction probabilities as a function of collision energy. This structure arises because the 1D collision complex lifetimes are principally determined by the relative velocity of the two heavy atoms in the system. If the two heavy atoms approach and separate in a time which corresponds to an integer number of intermediate H–L–H asymmetric vibrations (an even number of light atom exchanges) then no reaction will occur. If this time corresponds to a half number of vibrations (an odd number of light atom exchanges), then reaction will occur.

Less pronounced reactivity oscillations have also been seen in 3D quasiclassical trajectory calculations that use

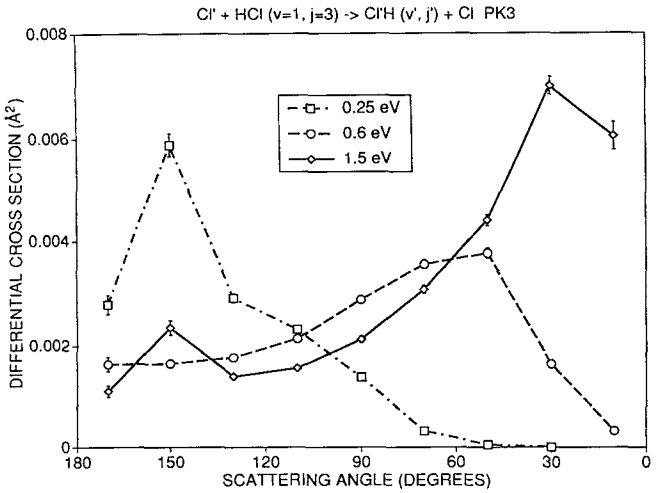

FIG. 8. Cl′+HCl(v=1, j=3)→Cl′H(v', j')+Cl product center-of-mass angular distributions calculated for reaction at 0.25, 0.6, and 1.5 eV collision energy.

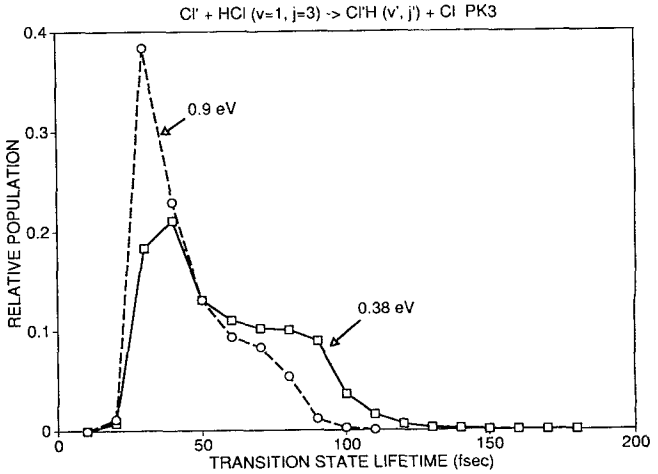

FIG. 9. Cl′+HCl(v=1, j=3) exchange reaction transition state lifetime distributions calculated for reaction at 0.38 and 0.9 eV collision energy. The transition state lifetime is defined in the text.

limited impact parameter and reactant orientation distributions, and it was suggested that reactivity oscillations could be probed in an oriented molecular beam scattering experiment.[19] However this type of experiment remains to be done. It is not known if reactivity oscillations will survive fully converged reactant conditions. If they do, then simpler experiments can be designed to probe this dynamically interesting phenomenon.

Our results show that reactivity oscillations are completely washed out in fully converged 3D QCT calculations of the Cl′+HCl(v=1, j=3)→Cl′H(v', j')+Cl reaction using the PK3 surface. An inspection of the energy dependence of total, partial, and differential cross sections, and energy partitioning for the reaction reveals no striking oscillatory structure. This result agrees, at least in part, with that predicted by Persky and Kornweitz.[19–23] In previous work these authors have shown that reactivity oscillations in backscattered differential cross sections are damped considerably if HCl reactant rotational states $>j=2$ are used. Our calculations used the $j=3$ state and so this may explain why we see no interesting structure. Persky and Kornweitz have also shown that oscillations are damped, but do not disappear, when 3D QCT calculations are done using a random distribution of reactant orientations but still confining the system to collide with small impact parameter.[20] We used a converged set of impact parameters and reactant orientations. It may be that extending the impact parameter range further dampens oscillations to the point that they cannot be seen. We are currently testing this latter hypothesis by performing fully converged 3D QCT calculations of the Cl+HCl(v=1, j=0) reaction.

The physical picture of reactivity oscillations in three dimensions is not as easy to visualize as the one dimensional case is. Studies which detail the exact dynamical phenomenon leading to oscillations in 3D cross sections have not been done. The only thing that is known with certainty is that the position and magnitude of the oscillations strongly depend upon the identity of the potential energy surface used in the calculations. Intuitively one would expect the oscillations to be correlated with the occurrence of multiple encounter collisions, and Persky and Kornweitz have noted that long-lived trajectories are more frequent on a surface which yields oscillations in back scattered differential cross sections than a surface which shown no oscillatory behavior.[19] As pointed out by the authors however, the sample size was limited and so no definite conclusion was made.

We have determined the transition state lifetime distributions and classified the exchange reaction trajectories as either direct or indirect to see if there is a correlation between multiple encounter collisions and presence (or absence) of reactivity oscillations. In these calculations we defined a trajectory to be at the transition state when both Cl–H bonds had lengths <2 Å. The time when the system first achieved the transition state criterion was noted. The Cl–H bond lengths were then monitored in each subsequent step of the trajectory and when one or more of the Cl–H bonds separated to a length >2 Å, denoting the end of the transition state, the time was noted. Some trajectories would react, separate, and then recollide. In these cases we noted the time when the complex last separated. The transition state lifetime was calculated by subtracting the initial time from the final time. Trajectories were classified as direct or indirect based upon the number of times the H atom was exchanged between the chlorine atoms in the system which was determined by monitoring the Cl′–H and H–Cl bond lengths during the course of the trajectory.

The QCT calculated transition state lifetime distributions are bimodal at all collision energies studied. Figure 9 shows the relative lifetime distributions calculated for the exchange reaction at 0.38 and 0.9 eV collision energy. Distributions at other collision energies are essentially identical and will not be presented. The 0.38 and 0.9 eV distributions have a fast component, which peaks around 30–40 fs, and a slow component, which shows up as a long tail

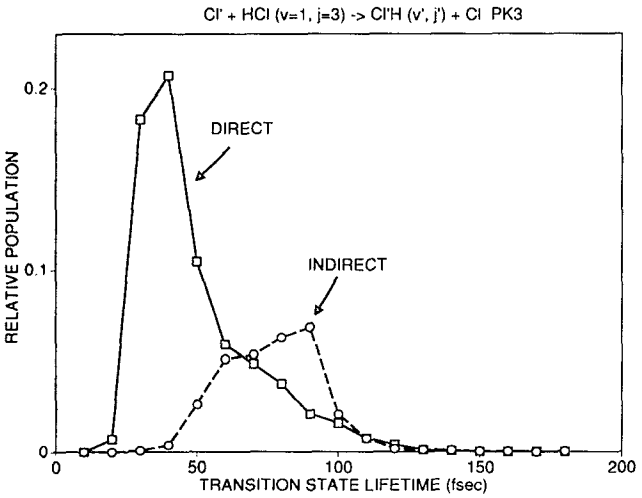

FIG. 10. Cl′+HCl(v=1, j=3) exchange reaction transition state lifetime distributions determined for the direct and indirect mechanisms. Reactant collision energy is 0.38 eV.

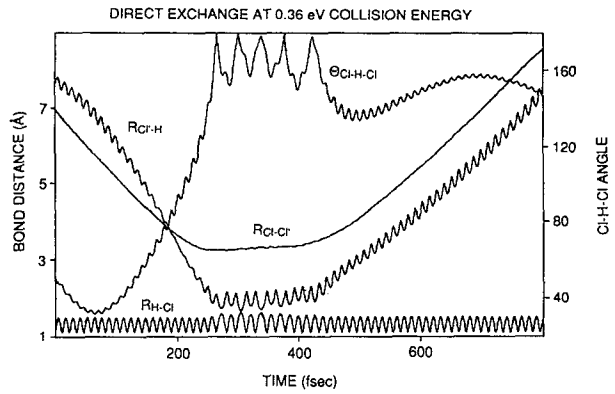

FIG. 11. An example of a long-lived Cl′+HCl(v=1, j=3) direct exchange reaction trajectory calculated at 0.36 eV collision energy. Potential anisotropy forces the collision complex to remain in a near collinear configuration (as indicated by the Cl–H–Cl angle of 180°) long after the initial H atom exchange has taken place.

with a maximum estimated to occur somewhere between 70 and 100 fs, depending upon the initial collision energy.

As expected, the fast component in these distributions corresponds to direct exchange, and the slow to indirect exchange. Proof for this is given in Fig. 10 which plots the relative transition state lifetime distributions calculated for 0.38 eV collision energy trajectories classified as direct or indirect exchange. The lifetimes seen in the indirect reaction channel span the range 10–180 fs, and the distribution peaks at 90 fs. The direct reaction distribution is strongly peaked at 40 fs, but interestingly enough, lifetimes as long as 180 fs are seen in this particular channel. These longer lifetime trajectories arise when forces, exerted by the potential energy surface, confine the reacting system to a collinear configuration so that the products cannot separate. An example of such a trajectory is shown in Fig. 11 which plots the H–Cl, Cl′–H, Cl′–Cl bond lengths, and Cl–H–Cl angle as a function of time for an observed direct exchange reaction (i.e., one H atom hand off) trajectory at 0.36 eV collision energy. The transition state lifetime of this direct exchange reaction trajectory is 170 fs.

An inspection of the QCT data show that 30% of the exchange reaction trajectories react via the indirect channel and that this percentage does not change, within the statistical error, over the range of collision energies studied. Since we did not observe any striking reactivity oscillations, we cannot say anything about the correlation between reactivity oscillations and the presence of long-lived collision complexes. But it may be that reactivity oscillations arise when there are changes in the percent of reaction that proceeds via the indirect mechanism at a particular collision energy.

We have closely examined the product vibrational, rotational, and angular distributions for the two channels and see only small differences. Table IV lists the branching ratios, $\langle v' \rangle$, $\langle j' \rangle_{v'=0}$, and $\langle j' \rangle_{v'=1}$ calculated for the direct and indirect exchange reactions at 0.38, 0.42, 0.8, and 0.9 eV collision energies. Since slight dips in backscattered (160°–180°) product differential cross sections were observed at 0.38 and 0.9 eV we chose to scrutinize these two energies in more detail. Extra data was generated for reaction at 0.42 and 0.8 eV for comparison purposes.

Table IV shows that there are only slight differences in product energy partitioning in the direct and indirect reaction mechanisms. As a general trend, the indirect mechanism appears to conserve vibration more strongly, i.e., the $\langle v' \rangle$ for the indirect channel is 0.8, the direct channel yields an $\langle v' \rangle$ of 0.7, but these differences are quite small and cannot be separated by monitoring the product vibrational state distributions. The indirect mechanism shows that rotation is more strongly conserved in the product $v'=1$ levels. For example, at 0.42 eV collision energy the indirect channel's $\langle j' \rangle_{v'=1}$ is 4.4, the direct channel is 6.2. But again these differences are minuscule and the product $v'=0$ and 1 rotational state distributions do not show any bimodal character.

The angular distributions for the 0.38 and 0.9 eV col-

TABLE IV. Product parameters for direct and indirect Cl+HCl exchange collisions.

	Direct				Indirect			
E_{col}	%	$\langle v' \rangle$	$\langle j' \rangle_{v'=0}$	$\langle j' \rangle_{v'=1}$	%	$\langle v' \rangle$	$\langle j' \rangle_{v'=0}$	$\langle j' \rangle_{v'=1}$
0.38	70	0.7	13.5	5.7	30	0.8	12.3	4.1
0.42	70	0.7	13.7	6.2	30	0.8	12.0	4.4
0.80	71	0.7	15.5	8.0	29	0.8	13.5	6.4
0.90	72	0.7	16.0	8.6	28	0.8	14.5	6.6

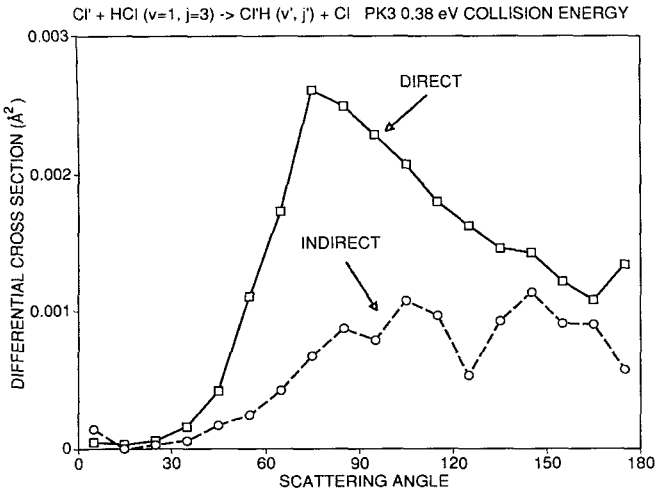

FIG. 12. Product center-of-mass angular distributions arising from the direct and indirect Cl′+HCl(v=1, j=3) exchange reaction mechanisms at a collision energy of 0.38 eV.

lision energy exchange reactions are plotted in Figs. 12 and 13, respectively. For reaction at the lower collision energies the results of Figs. 12 and 13 show that the direct channel concentrates most of its product into angles corresponding to sideways scattering. If one views the distributions in a relative sense though, one sees that the indirect reaction leads to an emphasis on backward scattering. The same can be said for reaction at the higher collision energies, except that in this case the direct reaction gives rise to a strongly forward scattered component, as expected for reaction at high collision energy.

It is interesting to note that indirect exchange mechanism on the PK3 surface primarily yields backward scattered products. This observation is quite different from that of Jakubetz *et al.*[15] who show that long lived Cl+HCl exchange reaction QCT trajectories on the BCMR surface are sideways scattered. The BCMR surface is different from the PK3 surface in that the former's bend potential is quite repulsive. The difference between our results and those of Jakubetz *et al.* emphasizes the extreme sensitivity that H+LH exchange reaction product angular distributions have toward bend potential anisotropy.

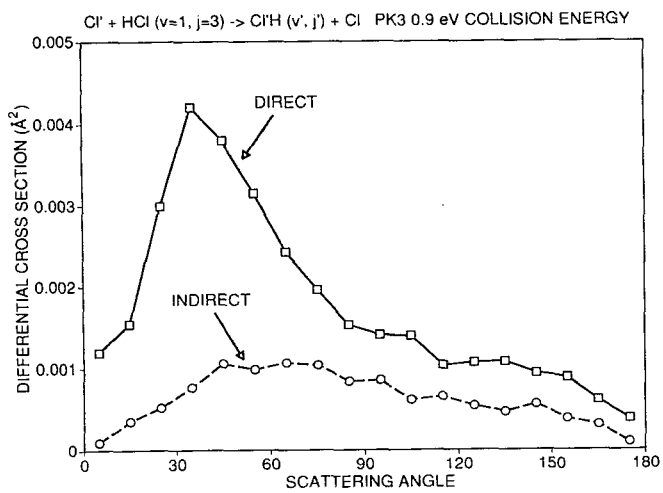

FIG. 13. Product center-of-mass angular distributions arising from the direct and indirect Cl′+HCl(v=1, j=3) exchange reaction mechanisms at a collision energy of 0.9 eV.

V. CONCLUSION

QCT calculations have been used to model Cl′+HCl(v=1, j=3)→Cl′H(v', j')+Cl exchange reaction dynamics on the PK3 potential energy surface over the 0–1.5 eV collision energy range. The reaction strongly conserves initial reagent vibrational excitation, independent of collision energy. Reagent rotational excitation is conserved at low collision energy, showing that kinematic constraints dominate, but at high collision energy the rotational state distributions broaden substantially, indicating a breakdown in the angular momentum selection rules. Product differential cross sections are also influenced by collision energy, but in an expected manner. At low collision energy backscattering dominates, at high collision energy the distribution shifts to the forward direction.

Reactivity oscillations were not seen even though detailed studies show that two mechanisms are important to the reaction dynamics. 70% of the reaction proceeds via direct exchange, 30% via indirect exchange. This ratio is independent of collision energy.

ACKNOWLEDGMENTS

Acknowledgment is made to the Donors of the Petroleum Research Fund, administered by the American Chemical Society, for support of this research.

[1] A. Weaver, R. B. Metz, S. E. Bradforth, and D. M. Neumark, J. Phys. Chem. **92**, 5558 (1988).
[2] R. B. Metz, T. Kitsopoulos, A. Weaver, and D. M. Neumark, J. Chem. Phys. **88**, 1463 (1988).
[3] R. B. Metz, T. Kitsopoulos, A. Weaver, S. E. Bradforth, and D. M. Neumark, J. Phys. Chem. **94**, 1377 (1990).
[4] I. M. Waller, T. N. Kitsopoulos, and D. M. Neumark, J. Phys. Chem. **94**, 2240 (1990).
[5] R. B. Metz, S. E. Bradforth, and D. M. Neumark, Adv. Chem. Phys. **81**, 1 (1992).
[6] G. Schatz, J. Chem. Phys. **90**, 3592 (1989).
[7] J. M. Bowman and B. Gazdy, J. Phys. Chem. **93**, 5129 (1989).
[8] B. Gazdy and J. M. Bowman, J. Chem. Phys. **91**, 4615 (1989).
[9] G. C. Schatz, J. Chem. Soc. Faraday Trans. **86**, 1729 (1990).
[10] J. M. Bowman, B. Gazdy, and Q. Sum, J. Chem. Soc. Faraday Trans. **86**, 1737 (1990).
[11] G. C. Schatz, D. Sokolovski, and J. N. L. Connor, Faraday Discuss. Chem. Soc. **91**, 17 (1991).
[12] G. C. Schatz, D. Sokolovski, and J. N. L. Connor, in *Advances in Molecular Vibrations and Collision Dynamics: Quantum Reactive Scattering*, edited by J. M. Bowman (JAI, Greenwich, Connecticut, 1993), Vol. II B.
[13] G. C. Schatz, D. Sokolovski, and J. N. L. Connor, J. Chem. Phys. **94**, 4311 (1991).
[14] J. N. L. Connor and W. Jakubetz, in Proceedings of the NATO Advanced Research Workshop, Colombella di Perugia, Italy 30 August–3 September, 1988, edited by A. Lagana.
[15] W. Jakubetz, D. Sokolovski, J. N. L. Connor, and G. C. Schatz, J. Chem. Phys. **87**, 6451 (1992).
[16] G. C. Schatz, Chem. Phys. Lett. **151**, 409 (1988).
[17] M. Baer and I. Last, Chem. Phys. Lett. **119**, 393 (1985).
[18] I. Last and M. Baer, J. Chem. Phys. **86**, 5534 (1987).
[19] A. Persky and H. Kornweitz, J. Phys. Chem. **91**, 5496 (1987).

[20] H. Kornweitz, M. Broida, and A. Persky, J. Phys. Chem. **93**, 251 (1989).
[21] A. Persky and H. Kornweitz, Chem. Phys. **130**, 129 (1989).
[22] H. Kornweitz and A. Persky, Chem. Phys. **132**, 153 (1989).
[23] A. Persky and H. Kornweitz, Chem. Phys. Lett. **159**, 134 (1989).
[24] K. Schulten and R. G. Gordon, J. Chem. Phys. **64**, 2918 (1976).
[25] J. T. Muckerman (private communication).
[26] R. D. Levine and R. B. Bernstein, in *Molecular Reaction Dynamics and Chemical Reactivity* (Oxford University, New York, 1987).
[27] P. M. Aker and J. J. Valentini, Isr. J. Chem. **30**, 157 (1990).